Multiplexed aptasensor based on metal ions labels for simultaneous detection of multiple antibiotic residues in milk

Falan Li, Yemin Guo, Xiangyou Wang, Xia Sun

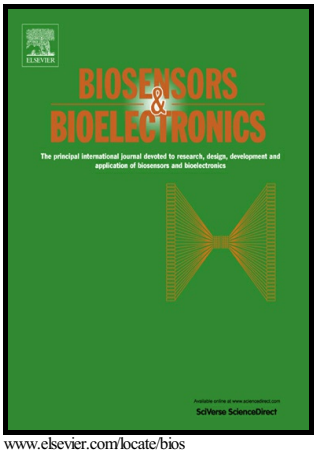

www.elsevier.com/locate/bios

PII: S0956-5663(18)30284-7
DOI: https://doi.org/10.1016/j.bios.2018.04.024
Reference: BIOS10420

To appear in: *Biosensors and Bioelectronic*

Received date: 20 March 2018
Revised date: 12 April 2018
Accepted date: 12 April 2018

Cite this article as: Falan Li, Yemin Guo, Xiangyou Wang and Xia Sun, Multiplexed aptasensor based on metal ions labels for simultaneous detection of multiple antibiotic residues in milk, *Biosensors and Bioelectronic,* https://doi.org/10.1016/j.bios.2018.04.024

Multiplexed aptasensor based on metal ions labels for simultaneous detection of multiple antibiotic residues in milk

Falan Li [a], Yemin Guo [b], Xiangyou Wang [a*,b], Xia Sun [b*]

[a]School of Engineering, Northeast Agricultural University, No. 59 Mucai Street Xiangfang District, Harbin 150000, Heilongjiang Province, P. R. China

[b]School of Agricultural Engineering and Food Science, Shandong University of Technology, No. 12 Zhangzhou Road, Zibo 255049, Shandong Province, P. R. China

Abstract

A dual-target electrochemical aptasensor was developed for the simultaneous detection of multiple antibiotics based on metal ions as signal tracers and nanocomposites as signal amplification strategy. Metal ions such as Cd^{2+} and Pb^{2+} could generate distinct differential pulse voltammetry (DPV) peaks. When targets were present, kanamycin (KAN) and streptomycin (STR) as models, the KAN aptamer (KAP) and STR aptamer (STP) were released from their complementary strands, with more change of Cd^{2+} and Pb^{2+} corresponding to peak currents. At the same time, complementary strand of KAP (cKAP) and STP (cSTP) were linked with

* Corresponding author: Professor Xiangyou Wang and Professor Xia Sun.

Tel.: +86 533 2780897

E-mail: wxy@sdut.edu.cn (X. Wang); sunxia2151@sina.com (X. Sun)

the poly (A) structure (cSTP-PolyA-cKAP) to increase their conformational freedom. Graphitized multi-walled carbon nanotubes ($MWCNT_{Gr}$) and carbon nanofibers-gold nanoparticles (CNFs-AuNPs) as a biosensor platform enhanced the surface area to capture a large amount of cSTP-PolyA-cKAP, thus amplifying the detection response. Under the optimal conditions, the aptasensor could detect KAN and STR as low as 74.50 pM and 36.45 pM respectively with the range from 0.1 to 100 nM and exhibited excellent selectively. Moreover, this aptasensor showed promising applications for the detection of other analytes by changing corresponding aptamers.

Keywords: *Multiplexed aptasensor; Simultaneous detection; Metal ions labels; Multiple antibiotic residues.*

1 Introduction

Antibiotics are a type of antimicrobial drug used in animals as growth promoters and also for the treatment of diseases (Ramezani et al., 2016; Pendela et al., 2009; Yan et al., 2016). However, when these antibiotics are overused, it will exist residues in animal derived food products, which can be hazardous for human health (Granja et al., 2009; Xue et al., 2016). Therefore, it is urgent to develop a kind of sensitive and quick assay to simultaneously detect multiple antibiotic residues in foods.

Currently, various methods have been reported to achieve the sensitive detection of antibiotic residues, *e.g.* LC-MS, TLC, HPLC, ELISA and immunoassays (Gbylik-Sikorska et al., 2013; Viñas et al., 2007; Gremilogianni et al., 2010; Xu et al., 2014b; Chen et al., 2008; Feng et al., 2016; Wei et al., 2012; Chen et al., 2013). However, one of the key aims for developing a detection method is to easily and rapidly measure the multiplex residues in food samples.

Recently, aptasensor has attracted considerable attention due to a good specificity,

usability and simplicity in diagnostics and detections (Ferapontova et al., 2008; Rahman et al., 2009). Aptamer is a short factitious RNA or single-stranded DNA sequence screened by an in vitro selection technique known as systematic evolution of ligands by exponential enrichment (Tuerk and Gold, 1990; Zhao et al., 2015), which specifically recognizes and binds to its pre-selected targets including small molecules, ions, proteins, and even whole cells (Tombelli et al., 2005; Gopinath et al., 2014; Ueyama et al., 2002; Evtugyn et al., 2013; Zhao et al., 2015; Cheng et al., 2007). According to previous reports, a variety of aptamers with high specificity for antibiotics has been screened and used (Zhou et al., 2013; Ghanbari et al., 2018).

One of the key aims of the simultaneous detection is to fabricate high-sensitive and distinguishable signal tags. Because the ability to simultaneously generate different dissolution peaks at different voltages, some metal ions, such as Cd, Pb, and Hg ions, have attracted considerable attentions for signal source (Feng et al., 2012; Xu et al., 2014a). Therefore, different aptamers labeled with different metal ions can be employed for multiple analytes simultaneous detection without interfering with each other.

For signal amplification, as we all know, nanomaterials play a key role on improving the electron transfer between aptamer and electrode surface (Janegitz et al., 2011; Du et al., 2010; Chen et al., 2012; Ansari et al., 2008). With their unique fiber structure, carbon nanofibers (CNFs) have a range of advantages, such as the high aspect ratio and good chemical stability (Barranco et al., 2010; Zhu et al., 2015; Su et al., 2005; Arshad et al., 2011; Moon and Farris, 2009). The long fiber nanostructure of CNFs makes them have a high specific surface area and helps deposit more gold nanoparticles (AuNPs). Graphitized multi-walled carbon nanotubes ($MWCNT_{Gr}$) have a high charge transfer property so that the current signals of the sensors are amplified and have a uniform interconnected network structure that enables them to immobilize more aptamer (Adegbenjo et al., 2017; Xue et al., 2017).

Considering the above findings, we developed a multiplexed aptasensor based on metal ions labels for simultaneous detection of multiple antibiotic residues. Herein, kanamycin (KAN) and streptomycin (STR) were used as models, and then KAN

aptamer (KAP) and STR aptamer (STP) were labeled with metal ions to realize simultaneous detection of KAN and STR. When KAN and STR were present, the interaction between antibiotic and aptamer led to the dissociation of dsDNA and resulted in more change of Cd^{2+} and Pb^{2+} corresponding to the peak currents. The complementary strand of KAP (cKAP) and STP (cSTP) were linked with the poly (A) structure (cSTP-PolyA-cKAP) to increase their conformational freedom. With the high charge transfer property of CNFs-AuNPs and $MWCNT_{Gr}$, the charge transfer rate of the aptasensor was obviously promoted. The proposed aptasensor has high sensitivity, and is reproducible and specific for multiple antibiotics. In addition, the aptasensor could be better applied for detecting antibiotic residues in real milk samples.

2 Experimental

2.1 Reagents

Kanamycin sulfate, streptomycin sulfate, tobramycin sulfate, sodium citrate, and chloroauric acid ($HAuCl_4$) were obtained from Sinopharm Chemical Reagent Co. CNFs and $MWCNT_{Gr}$ were obtained from DeKe-DaoJin Co. (Beijing, China). Bovine serum albumin (BSA) was purchased from BioDev-Tech. Co. (Beijing, China). STP, 5'-NH_2-GGGGTCTGGTGTTCTGCTTTGTTCTGTCGGGTCGT-3'; KAP, 5'-NH_2-AGATGGGGGTTGAGGCTAAGCCGA-3'; cKAP and cSTP linked with polyA structure (cSTP-PolyA-cKAP), 5'-NH_2-ACGACCCGACAGAACAAAGCAGAACACCAGACCCCAAAAAAAAAATCGGCTTAGCCTCAACCCCCATCT-3' were synthesized by Sangon Biotechnology (Shanghai, China).

2.2 Apparatus

SPCE was purchased from Zensor R&D Co. (Taiwan, TE100, China). Electrochemical measurements were carried out on an electrochemical workstation that was purchased from CH Instruments Co. (CHI 660D, China). The morphologies of the samples were characterized by a transmission electron microscope (TEM, FEI Tecnai G2F20S-TWIN, USA) and a scanning electron microscope (SEM, FEI Sirion

200, USA). Fourier transformation infrared (FT-IR) spectra were recorded using a FT-IR spectrometer from Thermo Electron Co. (Nicolet 5700, USA).

2.3 Preparation of CNFs-AuNPs

Prior to the preparation of AuNPs, all glassware were cleaned in freshly prepared aqua regia (HNO_3:HCl, 3:1), then rinsed thoroughly with ultrapure water and dried. The colloidal gold was prepared by dissolving 1% $HAuCl_4$ in H_2O with 3.95 mL of 1% trisodium citrate with vigorous stirring. When the reaction solution changed from light yellow to wine red, it indicated that the AuNPs had been successfully synthesized. Boiling was continued for 15 min, and then the solution was stirred until it cooled to room temperature. The nanoparticles colloidal solution and carbon fiber (1:1) were mixed to obtain the CNFs-AuNPs solution.

2.4 Labels of the aptamers with metal ions

CdS/KAP and PbS/STP nanochains were prepared as distinguishable signal probes (Dong et al., 2007). $Cd(NO_3)_2$ (0.2 mM, 100 mL) was added to the KAP solution acquiring a mixed solution-A and kept at 4 °C for 24 hours. 100 mL 0.2 mM Na_2S (water/ethanol, 1:1) was added to the mixed solution-A acquiring a mixed solution-B and kept at 4 °C for 24 hours. Then, $Cd(NO_3)_2$ aqueous solution (20 mM, 10 mL) was added to the mixed solution-B acquiring a mixed solution-C and incubated under 4 °C for 24 hours. Then, Na_2S (20 mM, 10 mL) was added to the mixed solution-C and incubated under 4 °C for 24 hours to obtain CdS/KAP nanochains. In addition, PbS/STP nanochains were synthesized based on the same abovementioned procedure except that $Cd(NO_3)_2$ was replaced by $Pb(NO_3)_2$.

2.5 Fabrication of the aptasensor

Firstly, the SPCE was cleaned by volt-amperometric cycling during 25 cycles in a 0.5 M H_2SO_4 solution (-1.5 V to +1.5 V, 100 mV/s) (Haddaoui and Raouafi, 2015), and then was washed with ultrapure water and dried in a stream of nitrogen gas. 10 µL of CNFs-AuNPs solution and 10 µL of $MWCNT_{Gr}$ suspension were successively added onto the SPCE surface and dried. Then, 10 µL of cSTP-PolyA-cKAP was

dropped onto the modified SPCE surface. 10 μL of the mixture solution of CdS-KAP and PbS-STP was added and incubated for 1.0 h to obtain an aptasensor interface for KAN and STR detection. Subsequently, to avoid nonspecific adsorption, 1% BSA was added and incubated for 2 h to block the remaining active sites. The obtained aptasensor was used to detect different concentrations of KAN and STR. Fig. 1 shows the preparation process for the aptasensor.

2.6 Detection of KAN and STR with the aptasensor

Differential pulse voltammetry (DPV) and cyclic voltammetry (CV) measurements were carried out in a compound solution of 0.1 M KCl and 5 mM $[Fe(CN)_6]^{3-/4-}$ which served as a redox probe. The stripping peaks of Cd^{2+} and Pb^{2+} could be clearly found at ~-0.68 V and ~-0.46 V. The resolved stripping peak signals related to the KAN and STR concentrations would be respectively measured.

2.7 Pretreatment of milk sample

Several milk samples were obtained from a local market. The samples were centrifuged for 10 min at 10,000 rpm to remove the interfering substances such as fat, after which the milk samples were collected by filtrating through a sterile Millipore membrane (0.22 μm). Subsequently, the milk samples were diluted 10 times with PBS (pH 7.5) for the detection by the proposed aptasensor.

3 Results and discussion

3.1 Characterization of the nanomaterials

The characterizations of different nanomaterials are shown in Fig. 2. A number of bright dots were observed on the highly entangled CNFs, indicating that CNFs-AuNPs were successfully prepared (Fig. 2, curve a). Fig. S1 show TEM and SEM images of the CNFs-AuNPs, as well as EDX analysis results of the elements C and Au. As shown in Fig. S1(c), C was almost completely covered on the surface and concentrated in the position of CNFs. This is because C was also the main component of the TEM copper net. Au was concentrated in the

position of CNFs, which indicated that the Au was distributed on the surface of the CNFs. In Fig. 2 (b), it could be seen that gold nanoparticles were attached to the surface of CNFs. The $MWCNT_{Gr}$ was highly entangled and exhibited a smoother morphology and highly ordered graphitic structure (Fig. 2, curve c). As shown in Fig. 2 (d), the measured outer diameter of $MWCNT_{Gr}$ was 40~70 nm and the inner diameter was approximately 10 nm.

3.2. Fourier transform infrared (FT-IR) spectroscopy

The CNFs-AuNPs and $MWCNT_{Gr}$ were further characterized by the FT-IR absorption spectra (Fig. S2). As shown in Fig. S2 (a), the major peaks were found at 3410, 1580, 1360, and 1070 cm^{-1}. These vibrations corresponded to -OH, -C=O, $-NO_2$, and O-H, respectively. The results indicated that the CNFs-AuNPs can be adsorbed to the electrode surface via electrostatic interaction. The $MWCNT_{Gr}$ exhibited strong vibration peaks at 3430, 1620, 1410, and 1050 cm^{-1} (Fig. S2 (b)). These stretching vibrations were attributed to -OH, -C=C, -C=N, and -C=O stretching, respectively. The results confirmed that $MWCNT_{Gr}$ and CNFs-AuNPs could be linked together and cSTP-PolyA-cKAP was adsorbed to the $MWCNT_{Gr}$/CNFs-AuNPs/SPCE surface by covalent binding.

3.3 Electrochemical characterization of the modified electrodes

As shown in Fig. 3, CVs were recorded during each immobilization step of the aptasensor manufacturing process. A pair of good reversible redox peaks was observed at the bare SPCE (A, curve a), indicating that $[Fe(CN)_6]^{3-/4-}$ had better redox property. When CNFs-AuNPs modified on the SPCE, the peak current of CV obviously increased (A, curve b), which indicated that CNFs-AuNPs had excellent charge transfer property. As shown in Fig. 3 (B), the increased of the peak current in CNFs-AuNPs/SPCE (B, curve d) was greater than that of CNFs/SPCE (B, curve b) and AuNPs/SPCE (B, curve c), which confirmed that the charge transfer property of CNFs-AuNPs was better than that of CNFs or AuNPs. When $MWCNT_{Gr}$ with excellent electrochemical behavior modified the electrode, the peak current further

increased (A, curve c). Because oligonucleotides could generate an insulating layer to hinder electron transfer, cSTP-PolyA-cKAP, CdS-KAP and PbS-STP were immobilized onto the electrode surface, and the redox peak currents were significantly reduced (A, curve d-e). The addition of BSA resulted in a further reduction in current, since BSA blocked the remaining active sites (A, curve f). The formation of the KAP-KAN (STP-STR) complex could hinder the electron transfer at the electrode interface so that the addition of KAN and STR resulted in a further decrease of the current signal (A, curve g). Briefly, these results demonstrated the sensing interface had been successfully fabricated.

3.4 Optimization of the analytical parameters

To achieve optimal sensing performance, cSTP-PolyA-cKAP concentration, pH, incubation time, and reaction time were optimized. An important parameter affecting the DPV response of the aptasensor was the concentration of cSTP-PolyA-cKAP. The response signal intensity of electrochemical aptasensor depended upon the selective binding of the KAP-KAN (STP-STR) complex. The concentrations of KAP and STP should be consistent with the concentration of cSTP-PolyA-cKAP. Thus, DPVs of the different concentrations of cSTP-PolyA-cKAP were recorded. As shown in Fig. 4 (a), the peak current difference (ΔI) increased with the increase of cKAP-PolyA-cSTP concentration, which was almost unchanged after reaching 5μM. Therefore, the cSTP-PolyA-cKAP concentration used in this work was 5 μM. The concentrations of KAP and STP were also selected at 5 μM depending on the pairing between oligonucleotides. The immobilization time of cSTP-PolyA-cKAP was also investigated in Fig. 4 (b). The ΔI increased rapidly with increasing immobilization time of cSTP-PolyA-cKAP to 60 min, because more cSTP-PolyA-cKAPs were attached on electrode. Then the ΔI growth leveled off because the immobilization number of cSTP-PolyA-cKAP reached saturation. Consequently, an optimized immobilization time of 60 min was applied in this experiment. The pH value was another important factor influencing the performance of the aptasensor, because it affected the activity of the biomaterials and the structure and properties of the

aptamer. The pH of the prepared aptasensor was optimized by immersing the aptasensor in different pH electrolytes. From Fig. 4 (c), it could be seen that the ΔI reached the maximum at pH 7.5. Therefore, the pH of the test solution was selected at 7.5 in this experiment. The incubation time for the aptamer was also optimized. After adding the aptamer, the ΔI of DPV for different incubation times is shown in Fig. 4 (d). The ΔI increased with the increase of incubation time, and there was almost no change over 60 min. Thus, the optimal incubation time was chosen as 60 min. To obtain a higher current response, the reaction time of the detection system was also optimized. It could be seen in Fig. 4 (e) that the ΔI of DPV increased with the extension of the reaction time and remained stable over 40 min, because the construction of the KAP-KAN (STP-STR) complex on the electrode surface reached saturation. Thus, 40 min was chosen as the reaction time.

3.5 Feasibility of the aptasensor and amplification performance of nanocomposites

In the construction of a multiplex electrochemical aptasensor, it is important to eliminate the cross-reactivity. In order to evaluate the cross-reactivity of the proposed aptasensor, DPV responses of two analytes were compared to those in presence of only one analyte. As shown in Fig. S3 (A), when the incubation solution contained one kind of analyte (curve a and b), the corresponding target analyte showed a higher current response, while the other basically did not show a current response. The results indicated that the detection of KAN and STR would not cause an interfere with each other. Moreover, the simultaneous addition of KAN and STR resulted in the simultaneous inrease of the corresponding currents (curve c), indicating that the cross-reactivity between the two analytes was negligible. The signal amplification was also confirmed by DPV responses. To verify the signal amplification effect of $MWCNT_{Gr}$ and CNFs-AuNPs, the current responses of the aptasensor were shown in Fig. S3 (B). The electrochemical signal of KAN+STR/BSA/CdS-KAP+PbS-STP/ cSTP-PolyA-cKAP/$MWCNT_{Gr}$/CNFs-AuNPs/SPCE (curve b) was 4.6 times higher than that of KAN+STR/BSA/CdS-KAP+PbS-STP/cSTP-PolyA-cKAP/SPCE (curve

a), which was because $MWCNT_{Gr}$ and CNFs-AuNPs as signal amplification strategy could accelerate electron transfer. Therefore, these results verified that the proposed aptasensor had significantly amplification ability.

3.6 Detection of KAN and STR

KAP and STP were labelled with PbS and CdS nanoparticles, and the peak currents of Pb^{2+} and Cd^{2+} moved for the sensitive and simultaneous detection of KAN and STR. As shown in Fig. 5 (A), the peak currents of Pb^{2+} and Cd^{2+} increased with the increase of KAN and STR concentration. The calibration curves displayed good linear relationships in the range from 0.1 to 100 nM with a regression equation of $y = 47.8526+15.5440x$ ($R^2 = 0.9870$) for KAN (Fig. 5 (B)), and a regression equation of $y = 46.5104+9.3681x$ ($R^2 = 0.9768$) for STR (Fig. 5 (C)), respectively. The lower detection limits (LODs) of the aptasensor were calculated to be 74.50 pM for KAN and 36.45 pM for STR using the formula 3 rb/m, where rb is the standard deviation of 11 parallel measurements of the blank solution ($rb_{KAN} = 0.38601$, $rb_{STR} = 0.11382$) and m is the slope of the curve in the linearity range of 0.1-100 nM ($m_{KAN} = 15.5440$, $m_{STR} = 9.3681$). The linear ranges and limits of detection of the aptasensor were better than those of some other methods (Table S1-S2) (Viñas et al., 2007; Xu et al., 2015; Qin et al., 2017; Chen et al., 2015; Zhou et al., 2014; Li et al., 2017; Li et al., 2014b; Qin et al., 2015; Ye et al., 2008; Xu et al., 2017; Yin et al., 2017) or electrochemical aptasensors in a single antibiotic measurement already reported (Table S3-S4) (Ramezani et al., 2016; Zhu et al., 2012; Qin et al., 2015; Liu et al., 2015; Sun et al., 2014; Li et al., 2014b; Bai et al., 2014; Mishra et al., 2015; Okoth et al., 2012; Zhou et al., 2013; Yin et al., 2017; Danesh et al., 2015). The lower limits of detection could be considered as follows: (1) CNFs-AuNPs and $MWCNT_{Gr}$ as the dual signal amplification strategies were promoted the electrode transfer rate of the aptasensor; (2) With an interconnection network structure of a larger specific surface area, $MWCNT_{Gr}$ enabled them to immobilize the aptamer.

3.7 Specificity, stability and reproducibility of the aptasensor

Specificity is one of the most important characteristics of an aptasensor. To investigate the specificity of the aptasensor, some interference experiments were performed by using the developed aptamer probe to detect KAN and STR in the presence of other antibiotics, such as gentamicin (G), tobramycin (T), and oxytetracycline (O). As displayed in Fig. 6 (a-b), even if concentrations of other target analogs (5 μM) were 100 times higher than those of KAN and STR (0.05 μM), the current differences due to the interfering substances were less than 7.6% of that without interferences (n=3). Those results indicated that the interference of high concentration target analogues was not very large. The low concentration of KAN (STR) and high concentration of other target analogs were respectively detected to further investigate the specificity of the aptasensor. As shown in Fig. 6 (c-d), the amperometric curve current response variations caused by the addition of high concentration of other target analogs were less than 6.8% for KAN and 8.9% for STR (n=3). The results showed that this multiplexed aptasensor had a high specificity because of its high binding specificity and affinity between the aptamers and their targets.

To investigate the reproducibility of the fabricated aptasensor, a fresh batch of five aptasensors were prepared and used to detect the mixture of KAN and STR. The relative standard deviations (RSDs) of the measurements were 3.16% for KAN and 4.84% for STR (n=5), which indicated that the designed electrochemical aptasensor in this study was precise and reproducible.

The aptasensor was stored in PBS (pH 7.5) at 4 °C to estimate the stability of the aptasensor. The average response current of the five aptasensors against KAN and STR solution decreased 8.67% and 9.51% after four weeks of storage (n=5), which indicated that the fabricated aptasensor had excellent stability. The stability of the aptasensor could be attributed to good stability of $MWCNT_{Gr}$ and AuNPs-CNFs and stability of the connection between aptamers and $MWCNT_{Gr}$.

3.8 Real sample analysis

The KAN and STR in milk samples were detected to achieve the feasibility study

of the aptasensor practical application. The milk sample was centrifuged (10,000 rpm, 10 min) and filtered through a sterile Millipore membrane (0.22 μm). Then, antibiotics (KAN and STR) at different concentrations were added to the filtered milk samples diluted 10 times with PBS (pH 7.5). The analytical results of the milk samples are shown in Table S5 and S6, and the recoveries were 92.51% to 108.95% for KAN and 91.75% to 106.36% for STR (n=3), and RSDs were in the ranges of 3.2-6.7% for KAN and 2.7%-5.3% for STR (n=3). Thus, it indicated that the aptasensor provided a promising application to detect multiple antibiotics in milk samples.

4 Conclusions

A selective, sensitive multiplexed electrochemical aptasensor was developed for simultaneous detection of multiple antibiotic residues, with KAN and STR as the models, based on $MWCNT_{Gr}$ and CNFs-AuNPs nanocomposites as amplification strategy and Cd^{2+} and Pb^{2+} as signal tracers. Notably, Cd^{2+} and Pb^{2+} produced distinguishable DPV peaks at differential electric voltage to realize simultaneous detection of multiple antibiotics. The signal amplification of $MWCNT_{Gr}$ and CNFs-AuNPs nanocomposites modified aptasensor was about 4.6 times compared with the absence of nanocomposites. The proposed aptasensor provided a promising application to the detection of multiple antibiotics in real milk samples. Furthermore, this work can be employed to detect other antibiotics by substituting of the appropriate aptamer, which provides a platform for the rapid and sensitive detection of multiplex antibiotics.

Acknowledgments

This work was supported by the National Natural Science Foundation of China (No.31471641, 31772068, 31701681), Special Project of Independent Innovation of Shandong Province (2014CGZH0703), Shandong Provincial Natural Science Foundation (ZR2014CM009, ZR2015CM016, ZR2016CM29, ZR2017BC001, ZR2014FL003), Key Research and Invention Program of Shandong Province

(2017GNC10119), Key Innovative project for 2017 Major Agriculture Application Technology of Shandong Province.

References

Adegbenjo, A.O., Olubambi, P.A., Potgieter, J.H., Shongwe, M.B., Ramakokovhu, M., 2017. Mater. Design. 128, 119-129.

Ansari, A.A., Kaushik, A., Solanki, P.R., Malhotra, B.D., 2008. Electrochem. Comm. 10, 1246-1249.

Arshad, S.N., Naraghi, M., Chasiotis, I., 2011. Carbon 49, 1710-1719.

Bai, X., Hou, H., Zhang, B., Tang, J., 2014. Biosens. Bioelectron. 56, 112-116.

Barranco, V., Lillo-Rodenas, M., Linares-Solano, A., Oya, A., Pico, F., Ibañez, J., Agullo-Rueda, F., Amarilla, J.M., Rojo, J.M., 2010. J. Phys. Chem. C. 114, 10302-10307.

Chen, H.W., Medley, C.D., Sefah, K., Shang, G.D., Tang, Z.W., Meng, L., Smith, J.E., Tan, W.H., 2008. Chem. Med. Chem. 3, 991-1001.

Chen, J., Li, Z., Ge, J., Yang, R., Zhang, L., Qu, L.B., Wang, H.Q., Zhang, L., 2015. Talanta 139, 226-232.

Chen, K.J., Lee, C.F., Rick, J., Wang, S.H., Liu, C.C., Hwang, B.J., 2012. Biosens. Bioelectron. 33, 75-81.

Chen, Y.P., Zou, M.q., Qi, C., Xie, M.X., Wang, D.N., Wang, Y.F., Xue, Q., Li, J.F., Chen, Y., 2013. Biosens. Bioelectron. 39, 112-117.

Cheng, A.K.H., Ge, B., Yu, H.Z., 2007. Anal. Chem. 79, 5158-5164.

Danesh, N.M., Ramezani, M., Emrani, A.S., Abnous, K., Taghdisi, S.M., 2015. Biosens. Bioelectron. 75, 123-128.

Dong, L.Q., Hollis, T., Connolly, B.A., Wright, N.G., Horrocks, B.R., 2007. Adv. Mater. 19, 1748-1751.

Du, D., Zou, Z., Shin, Y., Wang, J., Wu, H., Engelhard, M.H., Liu, J., Aksay, I.A., Lin, Y., 2010. Anal. Chem. 82, 2989-2995.

Evtugyn, G., Porfireva, A., Sitdikov, R., Evtugyn, V., Stoikov, I., Antipin, I., Hianik, T., 2013. Electroanal. 25, 1847-1854.

Feng, L.N., Bian, Z.P., Peng, J., Jiang, F., Yang, G.H., Zhu, Y.D., Yang, D., Jiang, L.P., Zhu, J.J., 2012. Anal. Chem. 84, 7810-7815.

Feng, X.B., Gan, N., Lin, S.C., Li, T.H., Cao, Y.T., Hu, F.T., Jiang, Q.L., Chen, Y.J., 2016. Sens. Actua. B: Chem. 226, 305-311.

Ferapontova, E.E., Olsen, E.M., Gothelf, K.V., 2008. J. Am. Chem. Soc. 130, 4256-4258.

Gbylik-Sikorska, M., Posyniak, A., Mitrowska, K., Bladek T., Zmudzki, J., 2013. Food. Addit. Contam. 30, 940-948.

Ghanbari, K., Roushani, M., 2018. Bioelechem. 120, 43-48.

Gopinath, S.C.B., Lakshmipriya, T., Awazu, K., 2014. Biosens. Bioelectron. 51, 115-123.

Granja, R.H.M.M., Niño, A.M.M., Zucchetti, R.A.M., Niño, R.E.M., Pate, R., Salerno, A.G., 2009. Anal. Chim. Acta. 637, 64-67.

Gremilogianni, A.M., Megoulas, N.C., Koupparis, M.A., 2010. J. Chromatogr. A. 1217, 6646-6651.

Haddaoui, M., Raouafi, N., 2015. Sens. Actua. B: Chem. 219, 171-178.

Han, C., Doepke, A., Cho, W., Likodimos, V., de la Cruz, A.A., Back, T., Heineman, W.R., Halsall, H.B., Shanov, V.N., Schulz, M.J., Falaras, P., Dionysiou, D.D., 2013. Adv. Funct. Mater. 23, 1807-1816.

Janegitz, B.C., Pauliukaite, R., Ghica, M.E., Brett, C.M.A., Fatibello-Filho, O., 2011. Sens. Actua. B: Chem. 158, 411-417.

Li, C., Zhang, Y.Y., Eremin, S.A., Yakup, O., Yao, G., Zhang, X.Y., 2017. Food. Chem. 227, 48-54.

Li, H., Sun, D.E., Liu, Y., Liu, Z., 2014a. Biosens. Bioelectron. 55, 149-156.

Li, R., Liu, Y., Cheng, L., Yang, C., Zhang, J., 2014b. Anal. Chem. 86, 9372-9375.

Liu, R., Yang, Z., Guo, Q., Zhao, J., Ma, J., Kang, Q., Tang, Y., Xue, Y., Lou, X., He, M., 2015. Electrochim. Acta. 182, 516-523.

Mishra, G.K., Sharma, A., Bhand, S., 2015. Biosens. Bioelectron. 67, 532-539.

Moon, S.C., Farris, R.J., 2009. Carbon 47, 2829-2839.

Munir, K.S., Zheng, Y., Zhang, D., Lin, J., Li, Y., Wen, C., 2017. Mater. Sci. Eng. A.

688, 505-523.

Pendela, M., Hoogmartens, J., Van Schepdael, A., Adams, E., 2009. J. Sep. Sci. 32, 3418-3424.

Qin, L., Zeng, G.M., Lai, C., Huang, D.L., Zhang, C., Xu, P., Hu, T.J., Liu, X.G., Cheng, M., Liu, Y., Hu, L., Zhou, Y.Y., 2017. Sens. Actua. B: Chem. 243, 946.

Qin, X., Guo, W., Yu, H., Zhao, J., Pei, M., 2015. Anal. Methods 7, 5419-5427.

Okoth, O.K., Yan, K., Zhang, J., 2017. Carbon 120, 194-202.

Rahman, M.A., Son, J.I., Won, M.S., Shim, Y.B., 2009. Anal. Chem. 81, 6604-6611.

Ramezani, M., Danesh, N.M., Lavaee, P., Abnous K., Taghdisi, S.M., 2016. Sens. Actua. B: Chem. 222, 1-7.

Su, D.S., Chen, X.W., Weinberg, G., Klein-Hofmann, A., Timpe, O., Hamid, S.B.A., Schlogl, R., 2005. Angew. Chew. Int. Ed. 44, 5488-5492.

Sun, X., Li, F., Shen, G., Huang, J., Wang, X., 2014. Analyst 139, 299-308.

Tombelli, S., Minunni, A., Mascini, A., 2005. Biosens. Bioelectron. 20, 2424-2434.

Tuerk, C., Gold, L., 1990. Science 249, 505-510.

Ueyama, H., Takagi, M., Takenaka, S., 2002. J. Am. Chem. Soc. 124, 14286-14287.

Viñas, P., Balsalobre, N., Hernández, C.M., 2007. Talanta 72, 808-812.

Wei, Q., Zhao, Y., Du, B., Wu, D., Li, H., Yang, M., 2012. Food. Chem. 134, 1601-1606.

Xu, T., Jia, X., Chen, X., Ma, Z., 2014a. Biosens. Bioelectron. 56, 174-179.

Xu, W., Wang, Y., Liu, S., Yu, J., Wang, H., Huang, J., 2014b. New. J. Chem. 38, 4931-4937.

Xu, X.X., Liu, D., Luo, L.J., Li, L.B., Wang, K., You, T.Y., 2017. Sens. Actua. B: Chem. 251, 564-571.

Xu, Y., Han, T., Li, X., Sun, L., Zhang, Y., Zhang, Y., 2015. Anal. Chim. Acta. 891, 298-303.

Xue, J.K., Liu, J., Wang, C.S., Tian, Y.P., Zhou, N.D., 2016. Anal. Methods 8, 1981-1988.

Xue, Y.D., Zheng, S.L., Sun, Z., Zhang, Y., Jin, W., 2017. Chemosphere 183, 156-163.

Yan, Z.D., Gan, N., Li, T.H., Cao, Y.T., Chen, Y.J., 2016. Biosens. Bioelectron. 78,

51-57.

Ye, B.C., Li, S.Y., Zuo, P., Li, X.H., 2008. Food. Chem. 106, 797-803.

Yin, J.L., Guo, W.J., Qin, X.L., Zhao, J., Pei, M.S., Ding, F., 2017. Sens. Actua. B: Chem. 241, 151-159.

Zhao, B., Wu, P., Zhang, H., Cai, C., 2015. Biosens. Bioelectron. 68, 763-770.

Zhou, N., Zhang, J., Tian, Y., 2014. Anal. Methods. 6, 1569-1574.

Zhou, N., Wang, J., Zhang, J., Li, C., Tian, Y., Wang, J., 2013. Talanta 108, 109-116.

Zhu, F., Zhao, J., Cheng, Y., Yan, X., 2015. J. Nanosci. Nanotechnol. 15, 3981-3986.

Zhu, Y., Chandra, P., Song, K.M., Ban, C., Shim, Y.B., 2012. Biosens. Bioelectron. 36, 29-34.

Figure Captions

Fig. 1. Schematic illustration of the preparation process for the aptasensor.

Fig. 2. TEM images: (a-b) CNFs-AuNPs; (c-d) $MWCNT_{Gr}$.

Fig. 3. CV: (A) (a) bare SPCE, (b) CNFs-AuNPs/SPCE, (c) $MWCNT_{Gr}$/CNFs-AuNPs/SPCE, (d) cSTP-PolyA-cKAP/$MWCNT_{Gr}$/ CNFs-AuNPs/SPCE, (e) CdS-KAP+PbS-STP/cSTP-PolyA-cKAP/$MWCNT_{Gr}$/ CNFs-AuNPs/SPCE, (f) BSA/CdS-KAP+PbS-STP/cSTP-PolyA-cKAP/ $MWCNT_{Gr}$/CNFs-AuNPs/SPCE, (g) KAN+STR/BSA/CdS-KAP+PbS-STP/ cSTP-PolyA-cKAP/$MWCNT_{Gr}$/CNFs-AuNPs/SPCE. (B) (a) bare SPCE, (b) CNFs/SPCE, (c) AuNPs/SPCE, (d): CNFs-AuNPs/SPCE.

Fig. 4. The influence of (a) cSTP-PolyA-cKAP concentration, (b) cSTP-PolyA-cKAP immobilization time, (c) pH of working, (d) incubation time, (e) reaction time. Error bars indicate the standard deviations (n = 3).

Fig. 5. (a) Simultaneous determination of different concentrations of KAN and STR, (b) calibration curve of KAN, (c) calibration curve of STR. Error bars are the standard deviations across three repetitive measurements, and data are fit using

linear regression.

Fig. 6. Selectivity assessment of the aptasensor. K : kanamycin, S : streptomycin , G: gentamicin, O: oxytetracycline and T: tobramycin. Error bars represent the standard deviations of three independent measurements.

Supplementary material

Fig. S1. (a) TEM image of CNFs-AuNPs; (b) SEM image of CNFs-AuNPs; EDX maps shown for (c) C, (d) Au distribution across the sample.

Fig. S2. The FT-IR transmission spectroscopy of (a) $MWCNT_{Gr}$; (b) CNFs-AuNPs.

Fig. S3. (A) DPV responses of (a) 0 nM KAN and 0.1 nM STR solution; (b) 0.1 nM KAN and 0 nM STR solution; (c) 0.1 ng/mL KAN and 0.1 nM STR in the aptasensor. (B) DPV responses of (a) KAN+STR/BSA/CdS-KAP+PbS-STP/cSTP-PloyA-cKAP/ SPCE; (b) KAN+STR/BSA/CdS-KAP+PbS-STP/cSTP-PloyA-cKAP/$MWCNT_{Gr}$/ CNFs-AuNPs/SPCE.

Table S1 Comparison with other KAN detection methods

Table S2 Comparison with other STR detection methods

Table S3 Comparison of various KAN electrochemical aptasensors

Table S4 Comparison of various STR electrochemical aptasensors

Table S5 Determination and recovery results of KAN in spiked milk samples

Table S6 Determination and recovery results of STR in spiked milk samples

Highlights

1) A multiplexed aptasensor based on metal ions labels has been used for simultaneous detection of multiple antibiotic residues.

2) CNFs-AuNPs and $MWCNT_{Gr}$ nanocomposites as signal amplification strategies are presented.

3) The aptasensor is successfully used for detecting multiple antibiotic residues in real milk samples.

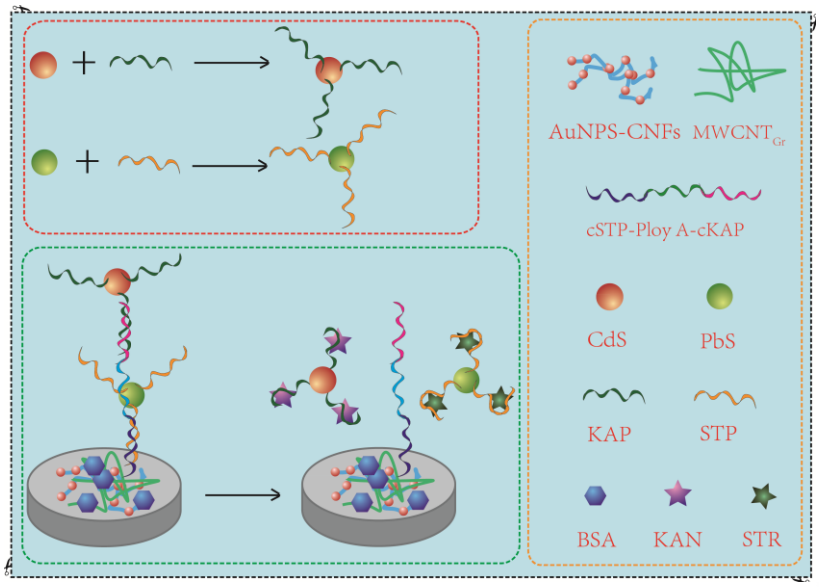

Fig. 1

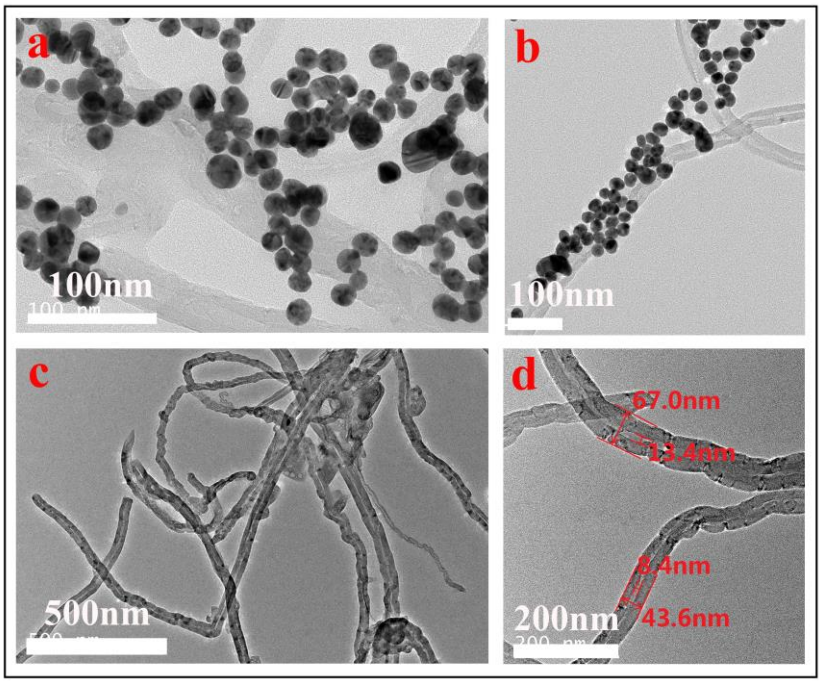

Fig. 2

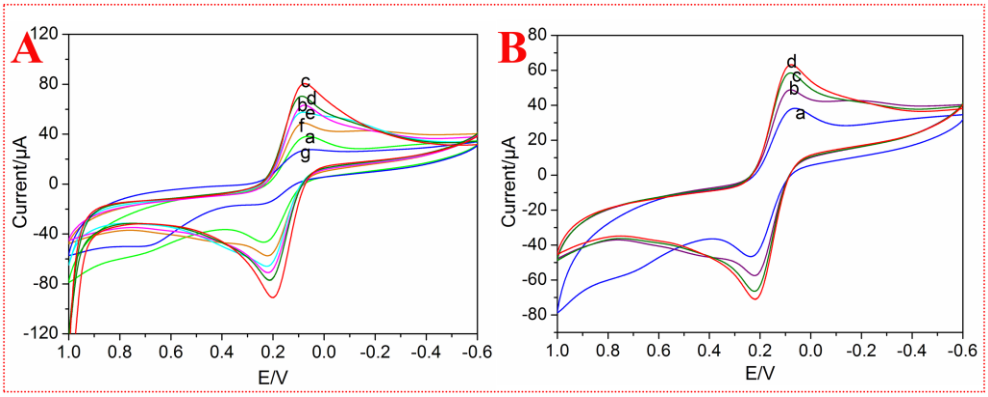

Fig. 3

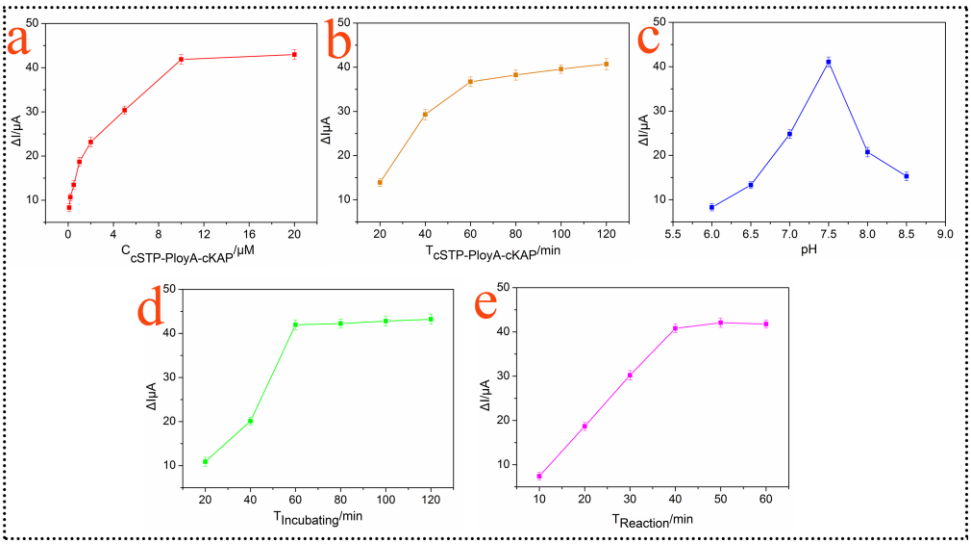

Fig. 4

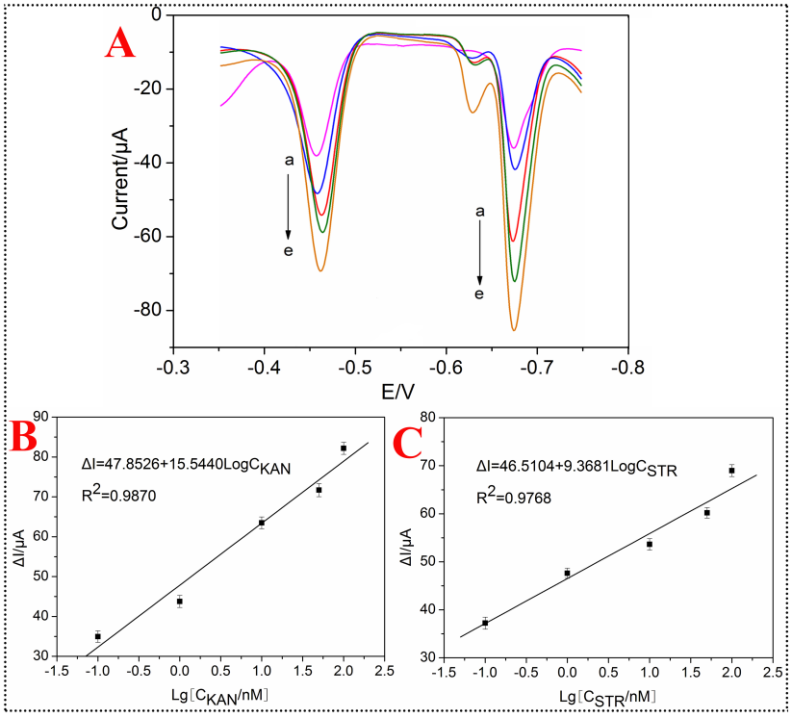

Fig. 5

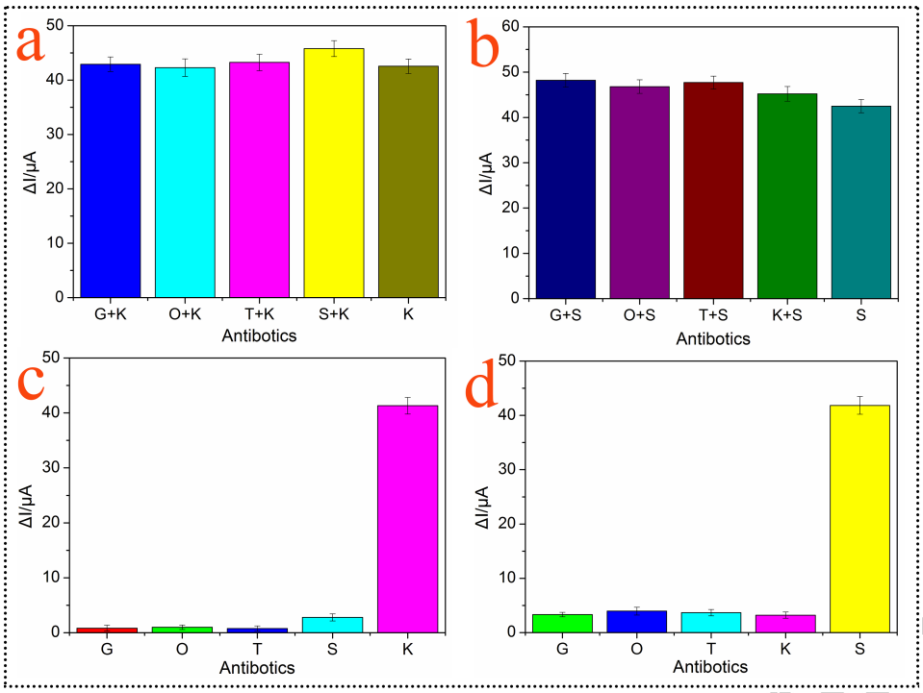

Fig. 6